Enhanced Raman Scattering from Nanoparticle-Decorated Nanocone Substrates: A Practical Approach to Harness In-Plane Excitation

Ying S. Hu,[†] Jaeseok Jeon,[#] Tae J. Seok,[#] Seunghyun Lee,[‡] Jason H. Hafner,[§,‡] Rebekah A. Drezek,[†,⊥] and Hyuck Choo[¶,#,*]

[†]Department of Bioengineering, [‡]Department of Chemistry, [§]Department of Physics and Astronomy, [⊥]Department of Electrical and Computer Engineering, Rice University, Houston, Texas 77005, [¶]The Molecular Foundry, Lawrence Berkeley National Laboratory, Berkeley, California 94720, and [#]Department of Electrical Engineering and Computer Sciences, University of California, Berkeley, California 94720

ABSTRACT We investigate surface-enhanced Raman scattering (SERS) from gold-coated silicon—germanium nanocone substrates that are decorated with 30-nm spherical gold nanoparticles (AuNPs). Finite-element simulations suggest that individual nanocones generate stronger electromagnetic enhancement with axial polarization (*i.e.*, polarization parallel to the vertical axis of the nanocones) than with transverse polarization (*i.e.*, polarization in the plane of the nanocone substrate), whereas the excitation in a typical Raman microscope is mainly polarized in the transverse plane. We introduce a practical approach to improve the SERS performance of the substrate by filling the valleys between nanocones with AuNPs. Simulations reveal an enhanced electric field at the nanoscale junctions formed between AuNPs and nanocones, and we explain this lateral coupling with a hybridization model for a particle-film system. We further experimentally verify the added enhancement by measuring SERS from trans-1,2-bi-(4-pyridyl) ethylene molecules absorbed onto the substrates. We report over one order-of-magnitude increase in SERS activities with the AuNP decoration (compared to the nanocone substrate without AuNPs) and achieve a spatially averaged enhancement factor of 1.78×10^8 at 785-nm excitation. Understanding and implementing the enhancing mechanism of structured metallic surfaces decorated with plasmonic nanoparticles open possibilities to substantially improve the SERS performance of the existing process-engineered substrates.

KEYWORDS: Raman scattering · SERS · nanocone substrate · gold nanoparticles · surface plasmon · plasmon hybridization · in-plane excitation

Surface-enhanced Raman scattering (SERS) has been extensively investigated on substrates formed by nanoparticles of various morphologies, compositions, and plasmonic properties.[1] Gold and silver nanoparticles possess unique optical properties due to their localized surface-plasmon resonance. Morphological features, such as sharp tips and edges, are believed to create strong spatially confined electric-field enhancement, which enhances Raman scattering of the molecules in the region. Mesoscopic nanoparticles with rich geometrical features have been investigated, such as dendritic nanostructures,[2] nanostars,[3,4] bipyramids,[5] meatball-like[6] and flower-like[7] particles. In addition to morphological features, nanoparticles of composite structures, such as core—shell nanoshells,[8−10] possess tunable plasmonic properties. These nanoparticles can be engineered to generate large electromagnetic field enhancement when the laser-excitation wavelength overlaps with the plasmon-resonance wavelength. A relatively new design explored core—satellite nanoparticle complexes, in which strong enhancement due to the synergistic and cascading effects was found.[11,12] Lately, bimetallic nanoparticles have gained research interest because of the synergism and plasmonic tunability of the metals.[1,13−18] Individual nanoparticles have also been assembled into conjugated dimers, trimers, and aggregates,[19,20] as well as one-dimensional nanoparticle chains,[21−23] nanodisk arrays,[24,25] two-dimensional nanoparticle arrays and clusters.[26−33] Large-scale three-dimensional structures have been created by depositing plasmonic nanoparticles into nonplasmonic templates.[34−37]

Concurrent with the plasmonic nanoparticle studies is a vast pool of literature that discusses the fabrication of process-engineered metallic substrates. Similar to nanoparticles, nanostructured metallic substrates create strong enhancement due to their plasmonic properties. Patterned nanostructures are often created by performing chemical and plasma etch on a supporting substrate and subsequently depositing a thin layer of gold onto the surface.[38−42] A design variant creates periodic impressions

*Address correspondence to hchoo@lbl.gov.

Received for review June 15, 2010 and accepted August 31, 2010.

Published online September 13, 2010.
10.1021/nn101352h

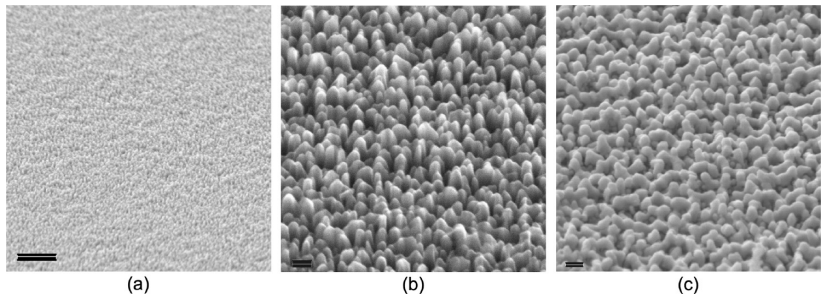

Figure 1. Scanning electron microscope images of (a) a low-magnification view of ordered nanostructures fabricated on the SiGe substrate, (b) a high-magnification view of the SiGe substrate shown in panel a, and (c) a side view taken at 40° of the SiGe substrate after deposition of 40 nm of gold (*i.e.*, the nanocone substrate). Scale bar is 1 μm in panel a and 100 nm in panels b and c.

instead of protruding nanostructures on thin gold films.[43,44]

An emerging new design utilizes plasmonic nanoparticles supported by a metallic structure that also exhibits surface plasmon properties. A recent paper reported a bimetallic nanocob structure, in which silver nanowires are coated with polymer layers embedded with 4-nm gold nanoparticles (AuNPs).[45] While two crossing nanowires with no AuNPs exhibited noticeable Raman signal only from the intersection point (where the gap distance is small), AuNP-decorated nanowires generated the Raman signal throughout the nanowires, at an intensity that is about 2 orders of magnitude stronger than that of the nondecorated silver wires.[45]

Inspired by the bistructured SERS substrates that exhibit high Raman activities, we report in this paper a simple and effective approach to improve SERS performance of a process-engineered nanocone substrate by decorating its surface with AuNPs. We have diagnosed the limitations of the substrate by simulating plasmonic properties of the AFM-characterized nanocone geometries at different excitation wavelengths and polarizations—the relatively weak enhancement exists with transversely polarized light. We show that this weak enhancement can be dramatically improved by adding AuNPs to the substrate and efficiently utilizing transversely polarized light. *Via* simulations, we demonstrate strong lateral coupling created by a 30-nm AuNP situated between a pair of nanocones. We experimentally verify the improved SERS performance by measuring and comparing Raman spectra of trans-1,2-bi-(4-pyridyl) ethylene (BPE) molecules absorbed onto the substrates with and without AuNPs.

RESULTS AND DISCUSSION

Fabrication of Nanocone Substrates. We fabricated the nanocone substrates by depositing a polycrystalline silicon−germanium (SiGe) layer on a silicon (Si) wafer, followed by plasma etch. The process produced ordered nanoscale peaks, as shown in Figure 1a,b. After dicing the wafer into 1 cm by 1 cm chips and attaching them to a handling Si-wafer, we evaporated a 40-nm gold layer onto the SiGe surface, producing the nanocone substrates shown in Figure 1c. We measured the thickness of the gold layer by characterizing the step height at the borderline between the areas covered and not covered by the gold layer on the handling Si-wafer. The deposition rate of the gold evaporation process is sensitive to incident angles, with maximum at normal incidence. As a result, the tips of the nano-

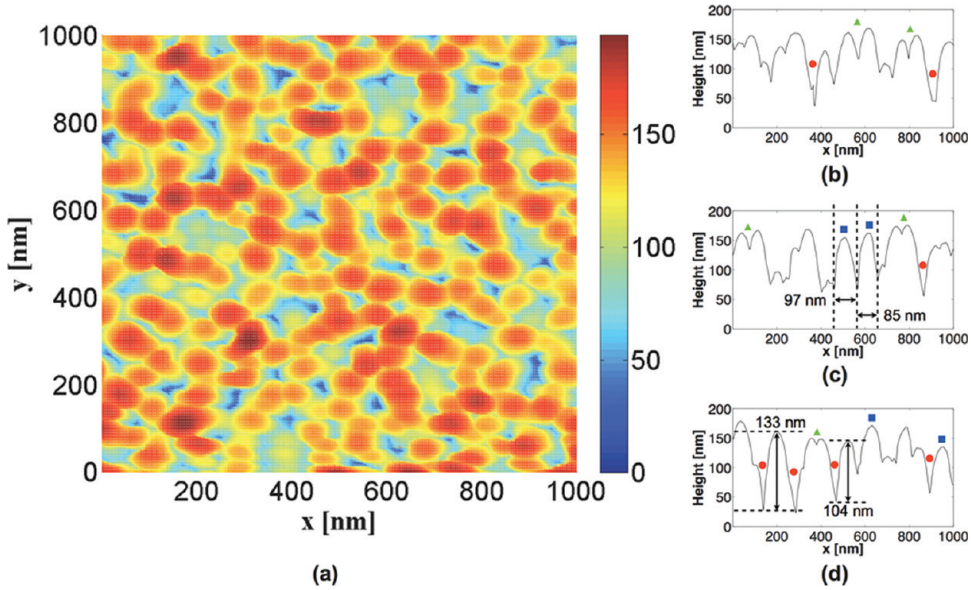

Figure 2. AFM height profile of the SiGe substrate before gold deposition. (a) Height profile of a two-dimensional scan, with color bar giving the height in nm. Individual line sectioning plots (b−d) show doublet peaks denoted by triangles, isolated single peaks denoted by blocks, and deep gaps between peaks denoted by circles.

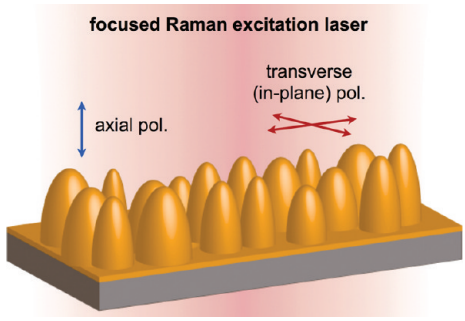

Figure 3. Illustration of the axial and transverse (in-plane) polarization of the Raman excitation light in relation to the SERS substrate.

scale peaks are covered by a 40-nm-gold layer, and the coating thickness tapers down toward the base. Side-view images taken at 40° are shown in Figure 1b,c and reveal the cone-like shapes of the nanocones.

Surface-Topology Analysis. To construct models that accurately represent the geometry of the nanocone, we characterized surface topologies of the nanocone substrate using atomic force microscopy (AFM) and scanning electron microscopy (SEM). We further estimated the effective gold surface area and the number of analyte molecules that could form a monolayer on the substrate. We later used this number to calculate the enhancement factor of the substrate.

An AFM scan of the height profile on a 1-μm^2 square area is displayed in Figure 2a. The *y* sectioning plots in Figure 2b−d show three common structures: doublet nanocones denoted by triangles, isolated single nanocones denoted by blocks, and nanocones with deep gaps denoted by circles. For SiGe nanocones, an average base radius of *ca.* 30−50 nm and a height of *ca.* 80−130 nm were measured. Dimensions of several nanocones are labeled in Figure 2c,d. (Also see Figure S1 in Supporting Information for high-magnification SEM images of the individual nanocones and Figure S2 for AFM cross-section analysis of the nanocones.) In our simulations, we employed a base radius of 40 nm (base width of 80 nm) and height of 100 nm. The average peak-to-peak separation varies between 60 and 150 nm. The AFM analysis of the surface revealed a nanocone density of 142 peaks/μm^2. Assuming all gold surfaces on the nanocones contribute to the SERS signal and by modeling nanocones as singlet cones with the dimensions given above, the effective gold surface area per μm^2 on the substrate is approximately 1.9 μm^2.

Simulations on the Polarization- and Wavelength-Dependent Characteristics of the Nanocone. Whereas Raman shifts are invariant with respect to the excitation energy, the strength and localization of the near-field electromagnetic (EM) enhancement of the SERS signal strongly depend on the excitation wavelength. This variation in strength and localization of the EM enhancement may cause the amplitude of certain Raman modes to be sensitive to excitation wavelength. In addition, the laser polarization plays a role in selectively exciting different modes depending on the geometry of the nanostructure. We examine herein the effects of two orthogonal polarizations of the excitation light: the excitation light polarized parallel to the vertical axis of the nanocone for axial polarization and perpendicular to the vertical axis for transverse polarization, as shown in Figure 3.

Figure 4 shows the magnitude of the normalized electric field when a nanocone is excited at four different wavelengths with axially polarized light (Figure 4a). The dimension of the SiGe nanocone is described previously. The gold coating is 40-nm thick on the tip and tapers down to 5 nm at the base. Strong EM enhancement is found at the tip of the nanocone and the distribution of the electric field varies at different wavelengths. For excitation at 543 nm (Figure 4a), the localized field is mainly focused at the gold tip of the nanocone; whereas for excitation at 1064 nm (Figure 4d), noticeable fields are developing inside the SiGe nanocone. We attribute this dependence on the excitation wavelength to plasmon hybridization of surface plasmons of the nanocone (*i.e.*, similar to the hybridization in a nanoshell).[46] The interplay between surface plasmons at the gold−air interface and at the SiGe−gold interface influences the localized electric field distribution.

The wavelength-dependent characteristic of the enhancement can also be observed when the excitation light is transversely polarized. Figure 5 shows this trait at the same wavelengths as are shown in Figure 4. Unlike with axial polarization, the nanocone exhibits low enhancement at the tip due to the geometrical symme-

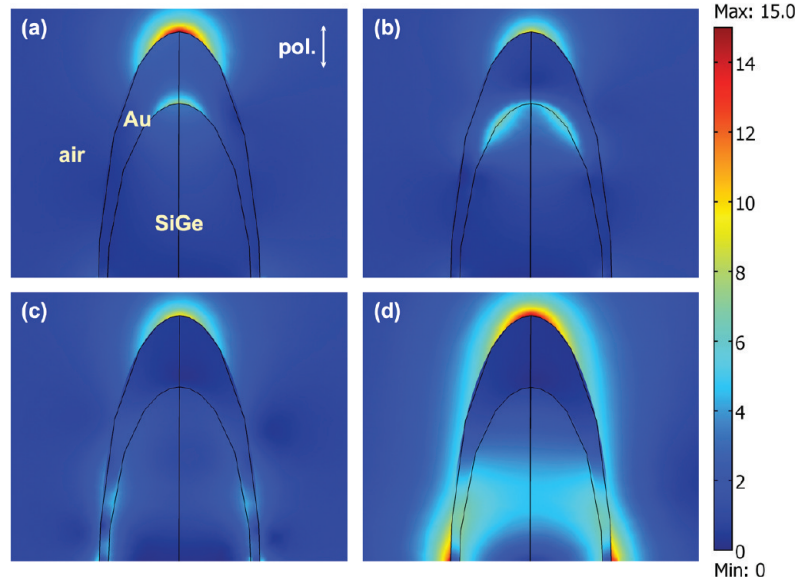

Figure 4. Normalized electric field of the nanocone with axial (vertical) excitation at four different wavelengths: (a) 543, (b) 633, (c) 785, and (d) 1064 nm.

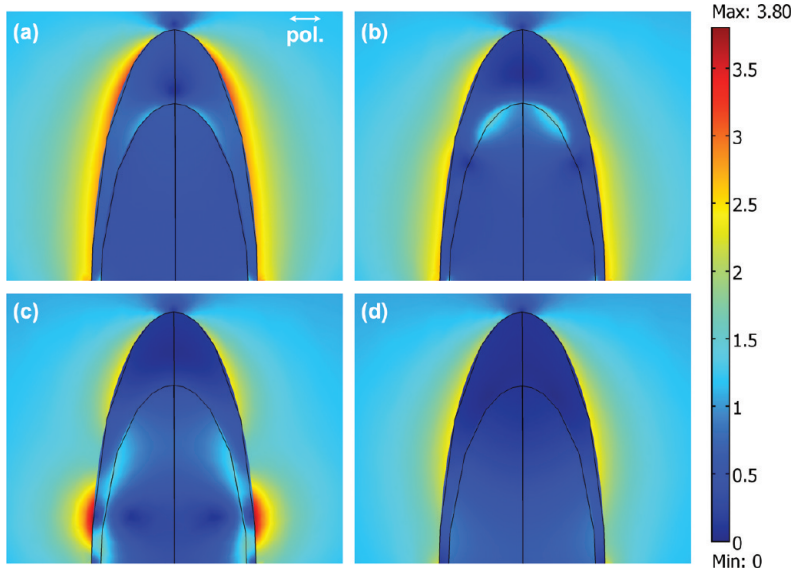

Figure 5. Normalized electric field of the nanocone with transverse (horizontal) excitation at four different wavelengths: (a) 543, (b) 633, (c) 785, and (d) 1064 nm.

try in the transverse direction. Figure 5c presents an interesting case where the section toward the base resonates at 785 nm, separately from the rest of the nanocone. This dipole-like plasmon resonance can be induced by the thin gold layer (~5 nm), which results in a strong coupling between the two aforementioned surface plasmons at 785 nm. This resonance wavelength blue shifts as the gold layer becomes thicker (*i.e.,* toward the tip of the cone). Despite the similar wavelength-dependent characteristic, the overall EM enhancement with transversely polarized light, as indicated by the color scale, is not as strong as with axially polarized light.

The relatively weak enhancement of the nanocones with in-plane excitation leaves space for improvement, because the majority of light is transversely polarized in a confocal setup where the laser light propagates perpendicularly to the sample substrate. An axial component of the focused light can exist only if the light is tightly focused to a point using a high NA objective (*i.e.*, the wavefront at the focal point has a slight curvature), or if the sample substrate is oriented oblique to the light. The EM enhancement from transversely polarized light improves if narrow nanocones are packed in close proximity with one another and form nanoscale gaps. We show in Figure 6 that a narrow gap between a pair of nanocones (Figure 6c) generates relatively strong enhancement, whereas a singlet (Figure 6a) and a doublet (Figure 6b) in general do not generate strong enhancement.

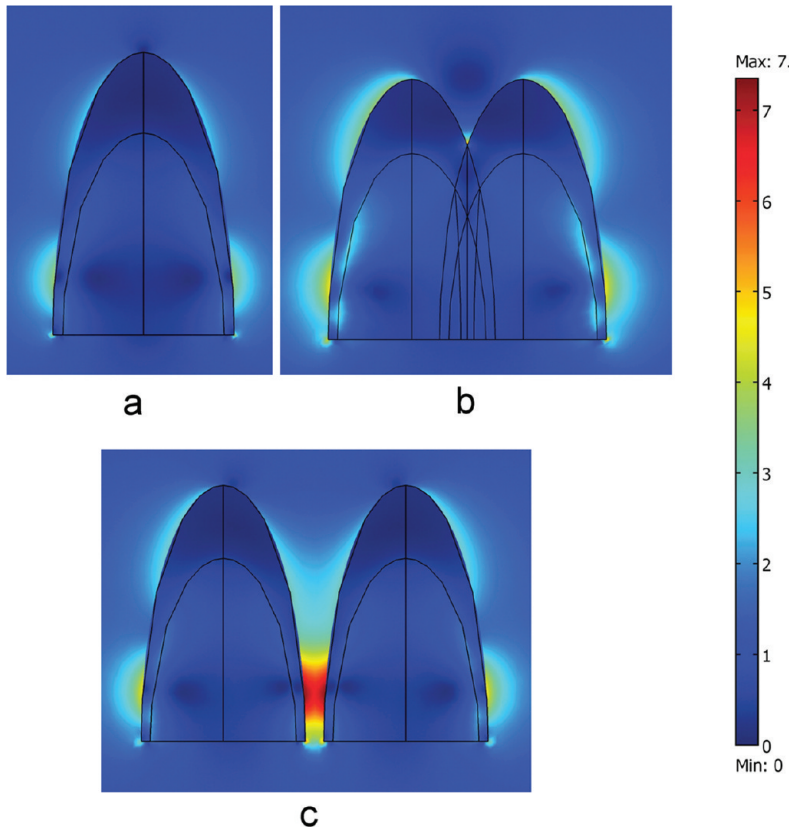

Figure 6. Normalized electric field of (a) a nanocone singlet, (b) a nanocone doublet with a peak-to-peak distance of 60 nm, (c) a nanocone pair with a peak-to-peak distance of 100 nm. Nanocones have the same dimension as previously described. Transverse excitation at 785 nm.

It is also noteworthy that the geometries and the surface morphology vary across the substrate. We show in Supporting Information (see Figure S3) plots of normalized electric field on nanocones with the base diameters and heights that vary up to ±25% from the geometry shown in Figures 4 and 5. We found that for axial polarization, the enhancement is affected by the tip radius; and for transverse polarization, the enhancement is more sensitive to the height of the nanocone than to its base width. The overall enhancing behavior of the nanocone, however, remains relatively insensitive to the variation of its dimensions. The simulations indicate that individual nanocones do not exhibit strong EM enhancement with transversely polarized light in comparison to axially polarized light. Thus, to improve the SERS performance of the substrate, we introduce plasmonic gold nanoparticles between nanocones to enhance the coupling efficiency to the transversely polarized light.

Lateral Coupling between Nanocones and AuNPs. AuNPs situated near nanocones create lateral nanoscale gaps that can

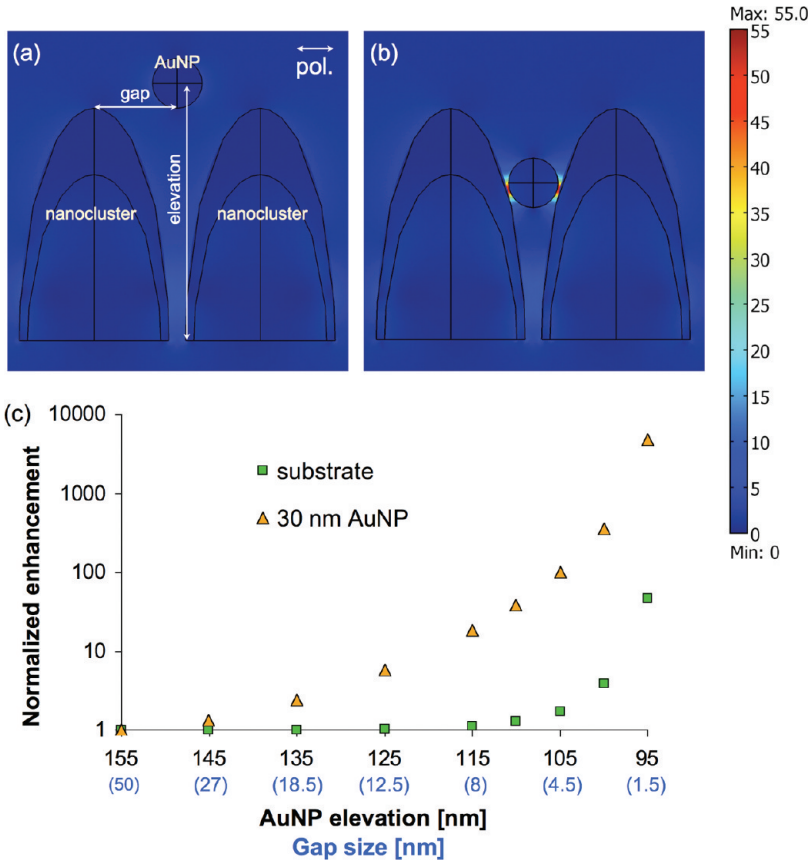

Figure 7. Normalized electric field distribution of a 30-nm AuNP located between a pair of nanocones 100-nm apart and the enhancement resulted from the coupling. The AuNP is situated at an elevation of (a) 155 and (b) 95 nm. Panel c shows the normalized enhancement *versus* particle elevation for the AuNP−nanocone system (gap size denoted in parentheses). The excitation light at 785 nm is transversely polarized.

be excited by transversely polarized light. Figure 7 shows the simulation results for an AuNP situated between two nanocones. Figure 7 panels a and b show the normalized electric field with the AuNP located at different elevations from the base of the nanocones. The excitation light is transversely polarized (along the gap) at 785 nm. The size of the gap between the AuNP and the nanocones is proportional to the vertical elevation of the AuNP from the substrate (shown in Figure 7a). Before the AuNP couples to the nanocones, a moderate enhancement of the electric field can be observed in the gap between the nanocones. When the AuNP and the nanocones are in the close proximity to each other, the coupling between the AuNP and the nanocones strengthens and creates strong hotspots (Figure 7b).

We interpret the coupling between the nanocones and the AuNP using a relevant particle-film system reported in the literature.[47−49] Briefly, the discrete plasmon modes of an AuNP couple with a continuum of the plasmon modes on a flat film. The superposition of the coupling between discrete and continuous modes creates virtual states. Surface charges on the nanoparticle and the nearby surface of the film generate large electric-field enhancement. In addition, image charges on the far side of the film contribute additional enhancement to the junction. Provided that the film is not too thin to support plasmons (*i.e.*, < 5 nm), a larger enhancement is generally observed on a thinner film.[48] In comparison to a flat film, a core−shell nanocone possesses a large number of discrete modes (due to its large surface area compared to AuNPs) instead of continuous modes. The hybridization between the nanoparticle and the nanocone creates a large number of localized discrete plasmon modes, some of which are shifted to the visible and near-infrared region. When the wavelength of a plasmon mode is in vicinity of the Raman excitation wavelength, a strong coupling can be induced. However, we note that the nanocone substrate employs a high-permittivity dielectric material ($\varepsilon_r = 14$ for SiGe), which induces a strong screening effect. The screening charges in the dielectric offset image charges on the gold-dielectric interface. For this reason, we suspect that the enhancement in the nanoparticle−nanocone junction is less sensitive to the thickness of the gold layer on the nanocone.

To quantify the added SERS enhancement, we integrate the electric field across the gold surfaces both on the substrate and on the AuNP. The EM enhancement, which is calculated as the fourth power of the electric field prior to the integration, is normalized by the values at the elevation of 155 nm, where the lowest point of the AuNP is at the same elevation as the peak of the nanocone and no visible coupling between the AuNP and the nanocones can be observed (Figure 7a). The normalized enhancement is plotted against AuNP elevation (or gap size) in Figure 7c. The enhancement increases both on the AuNP and on the nanocone substrate as the gap size decreases. Due to the relatively larger surface area of the nanocones with respect to the size of the hot spot, the EM field in the substrate is enhanced at a slower rate than its counterpart in the 30-nm AuNP. An enhancement over 10-fold is achieved on the substrate when the gap size is reduced to 1.5 nm.

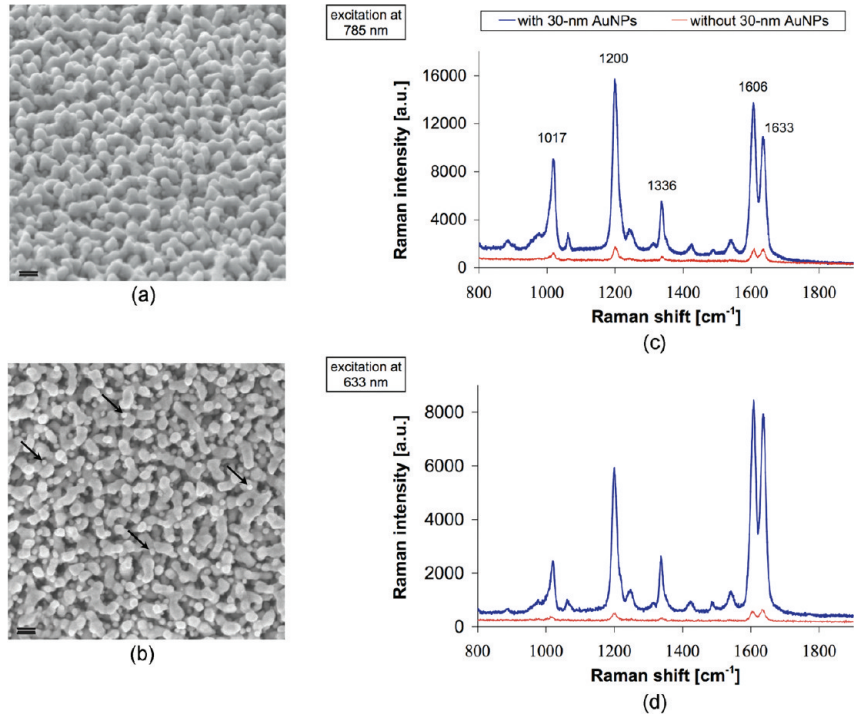

Figure 8. SEM images showing (a) a side view of the nanocone substrate prior to AuNP-deposition, (b) a top view of the nanocone substrate after AuNP-deposition, and SERS spectra from BPE molecules on the nanocone substrate with (blue) and without (red) 30-nm AuNPs with the excitation wavelength of (c) 785 and (d) 633 nm. Scale bar is 100 nm in panels a and b.

AuNP-Decorated Nanocone Substrates and SERS Measurements.

We performed experimental measurements to verify the improved SERS performance indicated by the simulation results. We decorated nanocone substrates using the 30-nm unconjugated colloidal gold solution in DI water purchased from Ted Pella (Redding, CA). The solution has a particle concentration of 2×10^{11} particles/mL. We applied 20 μL of the AuNP solution onto the substrate and let it dry in air. The area coated by the droplet occupied ~1/2 of the entire 1-cm^2 surface. On examining the AuNP-coated surface with an SEM, we found that AuNPs embedded evenly throughout the coated area and there were no large aggregates. Figure 8a shows a side view of the nanocone substrate before AuNP-decoration, and Figure 8b shows a top view of the nanocone substrate after AuNP-decoration (some AuNPs are indicated by the arrows).

We chose 50 μM BPE solutions to incubate all substrates. In general, studies indicate that the Raman intensity increases linearly at low concentrations of Raman molecules and gradually declines at higher concentrations. Van Duyne's group investigated cobalt phthalocyanine on rough Ag films and reported that the Raman intensity reaches its maximum at 10% monolayer coverage on rough substrates.[50] Meanwhile, for BPE molecules, increasing the molecular concentration results in self-quenching and causes the Raman intensity to decrease.[50,51] To estimate an optimal incubation time in conjunction with the concentration of BPE solution in order to obtain a submonolayer coating, we immersed seven nanocone substrates in 5-mL solutions of 50-μM BPE solutions for 1, 6, 12, 18, 24, 48, and 72 h, immediately followed afterward by SERS measurements. The intensity of the 1200 cm^{-1} mode increases approximately linearly from 1 to 24 h, and gradually levels off around 48 h (see Figure S5 in Supporting Information). The plot indicates that a 24-h incubation is likely to produce a submonolayer coverage. In light of this observation, we incubated the substrates in 5 mL of 50-μM BPE solutions for 24 h and blew dry the samples using N_2 gas.

We used a commercial Renishaw inVia Raman microscope for the SERS measurements. Figure 8 panels c and d show representative spectra obtained from the substrates with and without 30-nm AuNPs. Figure 8c corresponds to the excitation wavelength of 785 nm and Figure 8d corresponds to 633 nm. For the 633-nm laser, 5% of its power was coupled into the microscope and approximately 0.13 mW was delivered to the sample. For the 785-nm laser, 1% of its power was coupled into the microscope and approximately 0.29 mW was delivered to the sample. An integration time of 10 s was used. At both excitation wavelengths, the substrate coated with AuNPs exhibits substantially stronger Raman scattering than the substrate without AuNPs. Additionally, we note that among the five most prominent Raman modes of BPE molecules at 1017, 1200, 1336, 1606, and 1633 cm^{-1}, the amplitudes of the modes at 1200, 1606, and 1633 cm^{-1} appear to be sensitive to the excitation wavelength. At 785-nm excitation, the 1200-cm^{-1} peak is higher than the 1605- and 1634-cm^{-1} peaks; whereas at 633-nm excitation, the 1200-cm^{-1} peak is lower than the 1605- and 1634-cm^{-1} peaks. The relative change in amplitudes indicates a frequency-dependent nature of the SERS modes.

We use the 1200 cm^{-1} mode to characterize the enhancement Raman scattering of our substrates. Twenty individual SERS spectra were acquired from 10 different locations on the substrate. Within the AuNP-coated area, measurements were taken near the center to avoid densely packed AuNP aggregates that accumulated at the edges. SERS intensity of the 1200 cm^{-1} mode on the nanocone substrate before and after AuNP decoration has a standard deviation of 29% and 16% at 785 nm, and 22% and 18% at 633 nm, respectively. By comparing the intensity of 1200 cm^{-1} mode

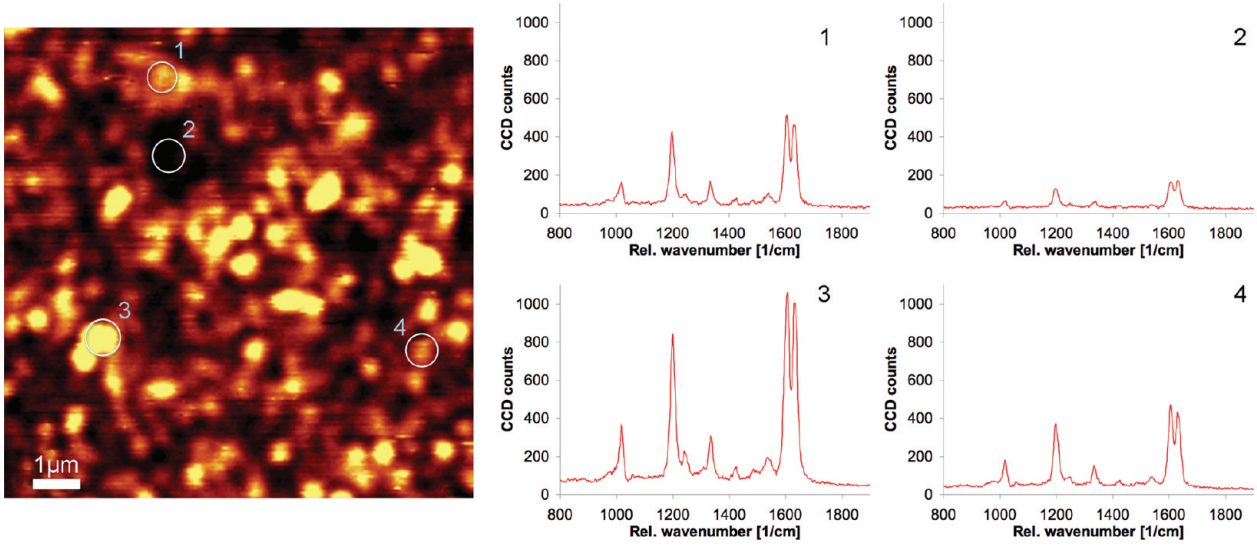

Figure 9. Raman scan of the 30-nm AuNP-coated nanocone substrate (left) and SERS spectra (right) from four locations labeled in the scan image. The excitation wavelength is 633 nm, and a 100×, 0.95 objective lens was used. For the Raman scan image, the 1200 cm^{-1} mode was captured by integrating intensities from 1178 to 1227 cm^{-1}.

from the same substrate before and after AuNP decoration, we found that the nanocone substrate decorated with AuNPs exhibited nearly 28 times stronger SERS activity at 785 nm compared to that of the nanocone substrate without AuNPs. Similar observation was made at 633 nm with an over 16-fold improvement.

A portion of the Raman enhancement after coating AuNPs to the nanocone substrate comes from the increased gold surface area from AuNPs. However, we prove here that this fraction is negligible in our experiments. From SEM images, such as Figure 8b, we estimate the particle density of the 30-nm AuNPs to be 76 particles/μm^2. The surface area added per μm^2 by AuNPs on the substrate is calculated by multiplying the particle density with the surface area of a 30-nm sphere, and it yields a merely 8% increase to the total surface area. Thus, the additional enhancement must originate from the lateral coupling between AuNPs and nanocones on the substrate.

While in simulations we study the EM enhancement and demonstrate formation of hotspots at nanoscale lateral junctions, some experimental observations are still unclear and require further study. For instance, the 1200-cm^{-1} mode from the nanocone substrate exhibits a frequency-dependent EM enhancement (*i.e.*, it is stronger than the 1600-cm^{-1} modes at 785-nm excitation, but weaker than the same modes at 633-nm excitation) both with and without AuNPs. Because EM theory suggests that all modes are equally amplified (*i.e.*, to the fourth power of the enhanced electric field), it cannot explain this mode-dependent enhancement. We experimentally observe that the AuNP-decorated nanocone substrate excites Raman modes in a nonuniform manner. For instance, the autofluoresence of the gold substrate, which appears as background in the SERS spectra, is distributed nonuniformly with respect to the Raman shifts. Therefore, a simple background subtraction may skew the amplitudes of the Raman modes. We expect future efforts to seek more accurate methods to scale the amplitude of each Raman mode with respect to the substrate background level.

Raman Scan and SERS Uniformity. The Raman spectra were acquired using a 50×, 0.55 objective and exhibit relatively good spatial enhancement uniformity for the combined substrate. We further examined the uniformity of the AuNP-decorated nanocone substrate by performing a Raman scan. To acquire the integrated Raman intensities across the substrate (*i.e.*, integrated intensities around the 1200 cm^{-1} mode), we employed a 100×, 0.95 objective. Figure 9 shows a representative scan of the AuNP-coated area on the nanocone substrate at 633-nm excitation along with Raman spectra sampled at four locations as indicated. Individual hotspots typically confined within 0.5−1 μm are clearly observed. Although these diffraction-limited hotspots do not allow us to resolve individual nanocone structures and AuNPs, the fact that they are distributed relatively uniformly over the nanocone substrate indicates that the AuNPs and the BPE are uniformly distributed over the nanocone substrate [this conclusion is also supported by the SEM image in Figure 8b]. With a lower NA objective (*i.e.*, 50×, 0.55), the Raman signal is spatially averaged and remains consistent over a large area of the substrate. Note that, if the AuNP coating was not uniform, large patches of enhancement (*i.e.*, bright areas in Figure 9) would be juxtaposed with large patches of nonenhancement (*i.e.*, dark areas in Figure 9).

Enhancement Factor. Using the 1200 cm^{-1} mode, we calculate the SERS enhancement factor (EF) of the 30-nm AuNP-decorated nanocone substrate at the excitation wavelength of 785 nm. The average background

intensity, mostly caused by the autofluorescence of the gold, was subtracted from the Raman spectrum to obtain the peak value. The effective area contributing to SERS is estimated by adding the surface area of the nanocones with the surface area of the AuNPs. From the details given in the sections discussing AFM and SEM characterization, the effective area is 1.9 times the laser spot size. The packing density of the BPE molecules is estimated to be 3.30×10^6 μm^{-2}, with the approximate area of a single molecule to be 30 Å^2.[52] We assumed 100% monolayer coverage of the surface by BPE molecules, which would lead to a more conservative estimate of EF due to the coating condition we used.

Prior to measuring Raman spectra from the neat solution, we determined the probe volume of the objective (50×, 0.55) using a gold nanocone substrate coated with BPE molecules as reference.[53] The probe volume is modeled as a cylinder with a diameter equal to the laser-focus spot size and height equal to the effective probe depth H_{obj}. The probe depth H_{obj} was measured by moving the substrate sample out of the focus plane at 1-μm increments and recording the Raman peak value at 1200 cm^{-1} at each position. Raman intensities were integrated over all positions and normalized by the maximum intensity at the focal plane, yielding $H_{obj} = 28.54$ μm.

We acquired neat spectra by placing an aliquot of 0.1 M BPE solution under the objective. The excitation light was first focused onto the backside of the sealing coverslip, then moved further into the solution. The excitation power at 785 nm and the integration time were chosen so that the clearly distinct 1200 cm^{-1} mode would be obtained in the neat BPE-Raman spectrum while the corresponding BPE-SERS measurement at the same settings would not saturate the detector.

The EF is calculated using

$$EF = \frac{I_{SERS}}{I_{neat}} \times \frac{N_{neat}}{N_{SERS}}$$

where I_{neat} and I_{SERS} represent the intensity of the neat and SERS signals of the 1200 cm^{-1} peak, and N_{neat} and N_{SERS} are the numbers of the BPE molecules contributing to the neat and SERS Raman intensities. As previously described, N_{neat} and N_{SERS} can be calculated from the effective volume and the effective surface area. Because we used the same measurement setup and excitation wavelength, the laser spot size is assumed to be identical, so it cancels out in the EF calculation. The spatially averaged EF is calculated to be 1.78×10^8.

CONCLUSIONS

From finite-element simulations, we show that individual nanocones on our process-engineered substrates do not generate strong enhancement with transversely polarized light, whereas the addition of gold nanoparticles creates lateral coupling to adjacent nanocones and harnesses transversely polarized light. The creation of nanoscale nanoparticle−nanocone junctions led to a relatively uniform enhancement of 1.78×10^8, over 1 order of magnitude stronger than that of the nanocone substrate alone. The use of plasmonic nanoparticles supported by plasmonic-structured metal surfaces is an efficient and practical approach. It has the potential to substantially improve the SERS sensitivity of the substrates designed with homogeneous structures and compositions.

METHODS

Experiments. The fabrication process of the nanocone substrates starts with the thermal oxidation followed by the deposition of rough poly-$Si_{40}Ge_{60}$ layer, as shown in Figure 10. The interplay of the surface roughness of the initial SiGe layer, the thickness of the protective Al_2O_3 layer, and the plasma etcher's incident-angle-sensitive etch rate/duration creates the topologies observed on the substrate.

Thermal oxidation was done in pyrogenic steam at 1000 °C for 1 h. The $Si_{40}Ge_{60}$ layer was deposited at 450 °C using low-pressure chemical deposition technique. A 20-nm Al_2O_3 film (200 cycles) was deposited onto the resulting surface at 300 °C using the Picosun SUNALE R-150 ALD reactor, a conformal atomic-layer-deposition system. To generate 20-nm layers, 200 cycles were required. A partially anisotropic dry etch of Al_2O_3 and the underlying SiGe layers was performed in a decoupled plasma system using BCl_3 and Cl_2 at 1000 W of RF power.

Unconjugated colloidal gold solutions were obtained from Ted Pella (Redding, CA, USA). The 30-nm gold colloidal solution concentration was 2.0×10^{11}. The AuNP solutions were stored at 4 °C and vortexed for 30 s before use. A 20 μL aliquot of gold colloidal solution was applied to the gold substrate, which was dried in air. The coated substrate was then incubated with 50-μM BPE (Sigma-Aldrich B52808) solution in methanol for 24 h. The substrate was blown dry with N_2 gas. The entire process is shown in Figure 10.

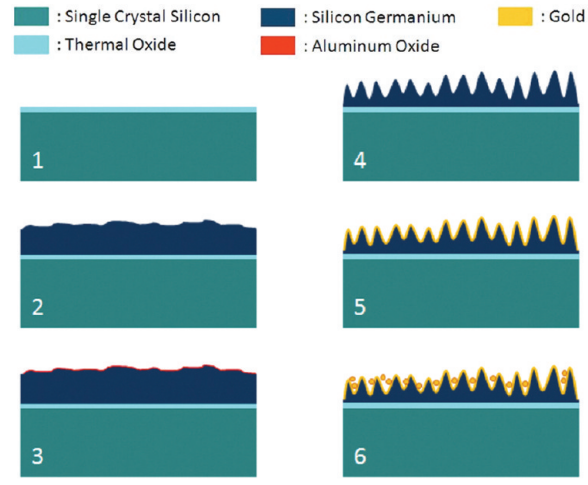

Figure 10. Fabrication process for the AuNP-coated nanocone substrate: (1) grow 450-nm thick thermal oxide on a silicon wafer; (2) deposit 1000-nm thick poly-$Si_{40}Ge_{60}$ at 450 °C; (3) deposit 20 nm of Al_2O_3; (4) perform a partially anisotropic dry etch for 1 min; (5) evaporate 20−150 nm of gold; (6) drop-apply AuNP colloidal solution.

Raman spectra were acquired by using a commercial Renishaw Raman microscope. A long working distance 50×, 0.55 objective lens was used for excitation and collection of the Raman spectrum. The Renishaw inVia Raman microscope allows the user to set certain percentage of the laser power to be sent to the microscope (1%, 5% , *etc.*). For the 500-mW laser at 785 nm, 1% of its power was sent to the microscope. For the 50-mW laser at 633 nm, 5% of its power was sent to the microscope. An integration time of 10 s was used for the spectral acquisition. The peak intensity at 1200 cm^{-1} was obtained after subtracting the averaged background level from the peak value.

Simulations. The surface topology of the SiGe substrate was profiled using a NanoScope IV MultiMode AFM (Veeco Instruments Inc., NY). A 1 μm^2 area was scanned with 512 steps in both the *x* and *y* directions. The height and base diameter of the nanocone features were determined from a scanned image of the height profile. The thickness of the gold layer at the peak of the nanostructure was set at 40 nm and was tapered down using a second degree Bézier curve to 10 nm at the base of the nanostructure. The dielectric constant of SiGe is 14.0 and that of gold was obtained from Johnson and Christy.[54] The ambient space in the simulation was assumed to be air with a dielectric constant of 1.0. The incident wave was set to be linearly polarized in the horizontal direction and propagated in the vertical direction (*i.e.*, normal to the nanostructure). The simulation was implemented using the RF module of COMSOL Multiphysics v3.5a.

Acknowledgment. The authors would like to thank P. Nordlander for discussion on the plasmon hybridization in the particle-film system, J. Bokor for discussion on polarization effects in confocal setups, A. Zayak for discussion on the chemical enhancement, A. Schwartzberg for the Raman scan, and S. Noelck for the preparation of the manuscript. This work was financially supported by the Welch Foundation Grant C-1598, DOE DE-FG02-97ER25308 and DARPA SERS S&T Program. The computational work was supported by the Shared University Grid at Rice University funded by NSF Grant EIA-0216467. Y. Hu acknowledges support from the DOE CSGF program.

Supporting Information Available: More details on characterization of the morphology of the nanocones using SEM and AFM, geometry effect on the electric-field distribution on the nanocones, and electric field enhancement in a nanocone doublet and a gap between two nanocones. This material is available free of charge *via* the Internet at http://pubs.acs.org.

REFERENCES AND NOTES

1. Ko, H.; Singamaneni, S.; Tsukruk, V. V. Nanostructured Surfaces and Assemblies as SERS Media. *Small* **2008**, *4*, 1576–1599.
2. Shamsaie, A.; Jonczyk, M.; Sturgis, J.; Robinson, J. P.; Irudayaraj, J. Intracellularly Grown Gold Nanoparticles as Potential Surface-Enhanced Raman Scattering Probes. *J. Biomed. Opt.* **2007**, *12*, 020502.
3. Esenturk, E. N.; Walker, A. R. H. Surface-Enhanced Raman Scattering Spectroscopy *via* Gold Nanostars. *J. Raman Spectrosc.* **2009**, *40*, 86–91.
4. Khoury, C. G.; Vo-Dinh, T. Gold Nanostars for Surface-Enhanced Raman Scattering: Synthesis, Characterization and Optimization. *J. Phys. Chem. C* **2008**, *112*, 18849–18859.
5. Lee, S.; Mayer, K. M.; Hafner, J. H. Improved Localized Surface Plasmon Resonance Immunoassay with Gold Bipyramid Substrates. *Anal. Chem.* **2009**, *81*, 4450–4455.
6. Wang, H.; Halas, N. J. Mesoscopic Au "Meatball" Particles. *Adv. Mater.* **2008**, *20*, 820–825.
7. Duan, G. T.; Cai, W. P.; Luo, Y. Y.; Li, Z. G.; Li, Y. Electrochemically Induced Flowerlike Gold Nanoarchitectures and Their Strong Surface-Enhanced Raman Scattering Effect. *Appl. Phys. Lett.* **2006**, *89*, 211905.
8. Hirsch, L. R.; Gobin, A. M.; Lowery, A. R.; Tam, F.; Drezek, R. A.; Halas, N. J.; West, J. L. Metal Nanoshells. *Ann. Biomed. Eng.* **2006**, *34*, 15–22.
9. Oldenburg, S. J.; Jackson, J. B.; Westcott, S. L.; Halas, N. J. Infrared Extinction Properties of Gold Nanoshells. *Appl. Phys. Lett.* **1999**, *75*, 2897–2899.
10. Jackson, J. B.; Halas, N. J. Surface-Enhanced Raman Scattering on Tunable Plasmonic Nanoparticle Substrates. *Proc. Natl. Acad. Sci. U.S.A.* **2004**, *101*, 17930–17935.
11. Gopinath, A.; Boriskina, S. V.; Premasiri, W. R.; Ziegler, L.; Reinhard, B. M.; Dal Negro, L. Plasmonic Nanogalaxies: Multiscale Aperiodic Arrays for Surface-Enhanced Raman Sensing. *Nano Lett.* **2009**, *9*, 3922–3929.
12. Chen, S. Y.; Lazarides, A. A. Quantitative Amplification of Cy5 SERS in "Warm Spots" Created by Plasmonic Coupling in Nanoparticle Assemblies of Controlled Structure. *J. Phys. Chem. C* **2009**, *113*, 12167–12175.
13. Gunawidjaja, R.; Kharlampieva, E.; Choi, I.; Tsukruk, V. V. Bimetallic Nanostructures as Active Raman Markers: Gold-Nanoparticle Assembly on 1d and 2d Silver Nanostructure Surfaces. *Small* **2009**, *5*, 2460–2466.
14. Rycenga, M.; Hou, K. K.; Cobley, C. M.; Schwartz, A. G.; Camargo, P. H. C.; Xia, Y. N. Probing the Surface-Enhanced Raman Scattering Properties of Au−Ag Nanocages at Two Different Excitation Wavelengths. *Phys. Chem. Chem. Phys.* **2009**, *11*, 5903–5908.
15. Pande, S.; Ghosh, S. K.; Praharaj, S.; Panigrahi, S.; Basu, S.; Jana, S.; Pal, A.; Tsukuda, T.; Pal, T. Synthesis of Normal and Inverted Gold−Silver Core−Shell Architectures in Beta-Cyclodextrin and Their Applications in SERS. *J. Phys. Chem. C* **2007**, *111*, 10806–10813.
16. Rivas, L.; Sanchez-Cortes, S.; Garcia-Ramos, J. V.; Morcillo, G. Mixed Silver/Gold Colloids: A Study of Their Formation, Morphology, and Surface-Enhanced Raman Activity. *Langmuir* **2000**, *16*, 9722–9728.
17. Hu, J. W.; Li, J. F.; Ren, B.; Wu, D. Y.; Sun, S. G.; Tian, Z. Q. Palladium-Coated Gold Nanoparticles with a Controlled Shell Thickness Used as Surface-Enhanced Raman Scattering Substrate. *J. Phys. Chem. C* **2007**, *111*, 1105–1112.
18. Bao, F.; Li, J. F.; Ren, B.; Yao, J. L.; Gu, R. A.; Tian, Z. Q. Synthesis and Characterization of Au@Co and Au@Ni Core−Shell Nanoparticles and Their Applications in Surface-Enhanced Raman Spectroscopy. *J. Phys. Chem. C* **2008**, *112*, 345–350.
19. Brousseau, L. C.; Novak, J. P.; Marinakos, S. M.; Feldheim, D. L. Assembly of Phenylacetylene-Bridged Gold Nanocluster Dimers and Trimers. *Adv. Mater.* **1999**, *11*, 447–449.
20. Wang, S. T.; Yan, J. C.; Chen, L. Formation of Gold Nanoparticles and Self-Assembly into Dimer and Trimer Aggregates. *Mater. Lett.* **2005**, *59*, 1383–1386.
21. Zeng, J.; Huang, J. L.; Lu, W.; Wang, X. P.; Wang, B.; Zhang, S. Y.; Hou, J. G. Necklace-like Noble-Metal Hollow Nanoparticle Chains: Synthesis and Tunable Optical Properties. *Adv. Mater.* **2007**, *19*, 2172–2176.
22. Lin, S.; Li, M.; Dujardin, E.; Girard, C.; Mann, S. One-Dimensional Plasmon Coupling by Facile Self-Assembly of Gold Nanoparticles into Branched Chain Networks. *Adv. Mater.* **2005**, *17*, 2553–2559.
23. Yang, Y.; Shi, J. L.; Tanaka, T.; Nogami, M. Self-Assembled Silver Nanochains for Surface-Enhanced Raman Scattering. *Langmuir* **2007**, *23*, 12042–12047.
24. Qin, L. D.; Zou, S. L.; Xue, C.; Atkinson, A.; Schatz, G. C.; Mirkin, C. A. Designing, Fabricating, and Imaging Raman Hot Spots. *Proc. Natl. Acad. Sci. U.S.A.* **2006**, *103*, 13300–13303.
25. Qin, L.; Banholzer, M. J.; Millstone, J. E.; Mirkin, C. A. Nanodisk Codes. *Nano Lett.* **2007**, *7*, 3849–3853.
26. Polavarapu, L.; Xu, Q. H. Water-Soluble Conjugated Polymer-Induced Self-Assembly of Gold Nanoparticles and Its Application to SERS. *Langmuir* **2008**, *24*, 10608–10611.
27. Kim, K.; Lee, H. B.; Lee, J. W.; Park, H. K.; Shin, K. S. Self-Assembly of Poly(ethylenimine)-Capped Au Nanoparticles at a Toluene−Water Interface for Efficient Surface-Enhanced Raman Scattering. *Langmuir* **2008**, *24*, 7178–7183.
28. Liao, J.; Bernard, L.; Langer, M.; Schonenberger, C.; Calame,

M. Reversible Formation of Molecular Junctions in 2d Nanoparticle Arrays. *Adv. Mater.* **2006**, *18*, 2444–2447.
29. Wang, H.; Levin, C. S.; Halas, N. J. Nanosphere Arrays with Controlled Sub-10-Nm Gaps as Surface-Enhanced Raman Spectroscopy Substrates. *J. Am. Chem. Soc.* **2005**, *127*, 14992–14993.
30. Hulteen, J. C.; Treichel, D. A.; Smith, M. T.; Duval, M. L.; Jensen, T. R.; Van Duyne, R. P. Nanosphere Lithography: Size-Tunable Silver Nanoparticle and Surface Cluster Arrays. *J. Phys. Chem. B* **1999**, *103*, 3854–3863.
31. Tsukruk, V. V.; Bliznyuk, V. N.; Visser, D.; Campbell, A. L.; Bunning, T. J.; Adams, W. W. Electrostatic Deposition of Polyionic Monolayers on Charged Surfaces. *Macromolecules* **1997**, *30*, 6615–6625.
32. Yan, B.; Thubagere, A.; Premasiri, W. R.; Zeigler, L. D.; Negro, L. D.; Reinhard, B. M. Engineered SERS Substrates with Multiscale Signal Enhancement: Nanoparticle Cluster Arrays. *ACS Nano* **2009**, *3*, 1190–1202.
33. Gopinath, A.; Boriskina, S. V.; Reinhard, B. M.; Dal Negro, L. Deterministic Aperiodic Arrays of Metal Nanoparticles for Surface-Enhanced Raman Scattering (SERS). *Opt. Express* **2009**, *17*, 3741–3753.
34. Tessier, P. M.; Velev, O. D.; Kalambur, A. T.; Rabolt, J. F.; Lenhoff, A. M.; Kaler, E. W. Assembly of Gold Nanostructured Films Templated by Colloidal Crystals and Use in Surface-Enhanced Raman Spectroscopy. *J. Am. Chem. Soc.* **2000**, *122*, 9554–9555.
35. Chan, S.; Kwon, S.; Koo, T. W.; Lee, L. P.; Berlin, A. A. Surface-Enhanced Raman Scattering of Small Molecules from Silver-Coated Silicon Nanopores. *Adv. Mater.* **2003**, *15*, 1595–1598.
36. Ko, H.; Tsukruk, V. V. Nanoparticle-Decorated Nanocanals for Surface-Enhanced Raman Scattering. *Small* **2008**, *4*, 1980–1984.
37. Kondo, T.; Nishio, K.; Masuda, H. Surface-Enhanced Raman Scattering in Multilayered Au Nanoparticles in Anodic Porous Alumina Matrix. *Appl. Phys. Express* **2009**, *2*, 032001.
38. Fan, J. G.; Zhao, Y. P. Gold-Coated Nanorod Arrays as Highly Sensitive Substrates for Surface-Enhanced Raman Spectroscopy. *Langmuir* **2008**, *24*, 14172–14175.
39. Geissler, M.; Li, K. B.; Cui, B.; Clime, L.; Veres, T. Plastic Substrates for Surface-Enhanced Raman Scattering. *J. Phys. Chem. C* **2009**, *113*, 17296–17300.
40. Linn, N. C.; Sun, C. H.; Arya, A.; Jiang, P.; Jiang, B. Surface-Enhanced Raman Scattering on Periodic Metal Nanotips with Tunable Sharpness. *Nanotechnology* **2009**, *20*, 225303.
41. Ruan, C. M.; Eres, G.; Wang, W.; Zhang, Z. Y.; Gu, B. H. Controlled Fabrication of Nanopillar Arrays as Active Substrates for Surface-Enhanced Raman Spectroscopy. *Langmuir* **2007**, *23*, 5757–5760.
42. Bora, M.; Fasenfest, B. J.; Behymer, E. M.; Chang, A. S.-P.; Nguyen, H. T.; Britten, J. A.; Larson, C. C.; Chan, J. W.; Miles, R. R.; Bond, T. C. Plasmon Resonant Cavities in Vertical Nanowire Arrays. *Nano Lett.* **2010**, *10*, 2832–2837.
43. Brolo, A. G.; Arctander, E.; Gordon, R.; Leathem, B.; Kavanagh, K. L. Nanohole-Enhanced Raman Scattering. *Nano Lett.* **2004**, *4*, 2015–2018.
44. Reilly, T. H.; Chang, S. H.; Corbman, J. D.; Schatz, G. C.; Rowlen, K. L. Quantitative Evaluation of Plasmon Enhanced Raman Scattering from Nanoaperture Arrays. *J. Phys. Chem. C* **2007**, *111*, 1689–1694.
45. Gunawidjaja, R.; Peleshanko, S.; Ko, H.; Tsukruk, V. V. Bimetallic Nanocobs: Decorating Silver Nanowires with Gold Nanoparticles. *Adv. Mater.* **2008**, *20*, 1544–1549.
46. Prodan, E.; Radloff, C.; Halas, N. J.; Nordlander, P. A Hybridization Model for the Plasmon Response of Complex Nanostructures. *Science* **2003**, *302*, 419–422.
47. Le, F.; Lwin, N. Z.; Steele, J. M.; Kall, M.; Halas, N. J.; Nordlander, P. Plasmons in the Metallic Nanoparticle—Film System as a Tunable Impurity Problem. *Nano Lett.* **2005**, *5*, 2009–2013.
48. Nordlander, P.; Le, F. Plasmonic Structure and Electromagnetic Field Enhancements in the Metallic Nanoparticle−Film System. *Appl. Phys. B* **2006**, *84*, 35–41.
49. Le, F.; Lwin, N. Z.; Halas, N. J.; Nordlander, P. Plasmonic Interactions between a Metallic Nanoshell and a Thin Metallic Film. *Phys. Rev. B* **2007**, *76*, 165410.
50. Zeman, E. J.; Carron, K. T.; Schatz, G. C.; Vanduyne, R. P. A Surface Enhanced Resonance Raman-Study of Cobalt Phthalocyanine on Rough Ag Films—Theory and Experiment. *J. Chem. Phys.* **1987**, *87*, 4189–4200.
51. Chaney, S. B.; Shanmukh, S.; Dluhy, R. A.; Zhao, Y. P. Aligned Silver Nanorod Arrays Produce High Sensitivity Surface-Enhanced Raman Spectroscopy Substrates. *Appl. Phys. Lett.* **2005**, *87*, 031908.
52. Felidj, N.; Aubard, J.; Levi, G.; Krenn, J. R.; Salerno, M.; Schider, G.; Lamprecht, B.; Leitner, A.; Aussenegg, F. R. Controlling the Optical Response of Regular Arrays of Gold Particles for Surface-Enhanced Raman Scattering. *Phys. Rev. B* **2002**, *65*, 075419.
53. Smythe, E. J.; Dickey, M. D.; Bao, J. M.; Whitesides, G. M.; Capasso, F. Optical Antenna Arrays on a Fiber Facet for *in Situ* Surface-Enhanced Raman Scattering Detection. *Nano Lett.* **2009**, *9*, 1132–1138.
54. Johnson, P. B.; Christy, R. W. Optical Constants of the Noble Metals. *Phys. Rev. B* **1972**, *6*, 4370–4379.